Journal of Asian Ceramic Societies

ISSN: (Print) (Online) Journal homepage: https://www.tandfonline.com/loi/tace20

Assessment of crystalline phase change and porosity by Rietveld refinement on lightweight cullet and paper ash glass-ceramic

K. Abu-Samah, M.R. Sahar, M. Yusop, F. Mohd-Noor, M.F. Omar, R. Zainal & D.N. F. Abdul Halim

To cite this article: K. Abu-Samah, M.R. Sahar, M. Yusop, F. Mohd-Noor, M.F. Omar, R. Zainal & D.N. F. Abdul Halim (2020) Assessment of crystalline phase change and porosity by Rietveld refinement on lightweight cullet and paper ash glass-ceramic, Journal of Asian Ceramic Societies, 8:3, 653-661, DOI: 10.1080/21870764.2020.1772528

To link to this article: https://doi.org/10.1080/21870764.2020.1772528

JOURNAL OF ASIAN CERAMIC SOCIETIES
2020, VOL. 8, NO. 3, 653–661
https://doi.org/10.1080/21870764.2020.1772528

THE CERAMIC SOCIETY OF JAPAN
THE KOREAN CERAMIC SOCIETY
Taylor & Francis
Taylor & Francis Group

FULL LENGTH ARTICLE

OPEN ACCESS Check for updates

Assessment of crystalline phase change and porosity by Rietveld refinement on lightweight cullet and paper ash glass-ceramic

K. Abu-Samah, M.R. Sahar, M. Yusop, F. Mohd-Noor, M.F. Omar, R. Zainal and D.N. F. Abdul Halim

Advance Optical Material Research Group, Department of Physics, Faculty of Science, UniversitiTeknologi Malaysia, Skudai, Malaysia

ABSTRACT

Lightweight glass-ceramic from waste material consists of (x) paper ash- (80-x) cullet – 20 Kaolin clay where (10 ≤ x ≤ 30 weight %) are sintered at 900°C, 1000°C and 1100°C using conventional solid-state reaction technique. The influence of composition and sintering temperature on density, crystalline phase, porosity and surface pore morphology was studied. The crystal symmetry, space group and unit cell dimensions which are executed from XRD data are analyzed using SmartLab Studio II Powder XRD software. Meanwhile, the lattice parameter, cell volume, theoretical densities and porosity were estimated by **Rietveld refinement** method. The results reveal that all parameters exhibit a temperature-dependent character, as the temperature is increased, the density decreases and porosity increases due to bloating effects. It is also found out that the glass-ceramic compose of 25 paper ash –55 cullet-20 Kaolin clay, sintered at 900°C exhibits an optimum characteristic of the sample density reached optimum because of vitrification between cullet glass, paper ash and kaolin clay to form liquid phase which promotes adhesion and polymerization. It is observed that the surface morphology of the sample is affected by the crystallization process during sintering.

ARTICLE HISTORY
Received 9 December 2019
Accepted 17 May 2020

KEYWORDS
Waste material; wollastonite; structural properties; porosity; Rietveld refinement

1. Introduction

The waste generated especially in big cities is expected to continue rising up mainly due to the uncontrolled waste production, immature recycling, limited landfill sites and fewer infrastructures in biological treatment. Waste management suddenly becomes a big issue [1]. In view of this scenario, practical solutions are to convert waste to valuable industrial products like glass-ceramic material. Sintered-crystalized glass-ceramics are significant alternatives for low cost and energy-saving production. Consequently, it could not only eliminate the potential hazards due to the bad environment but also solidifying chemical pollutions in certain areas. In the liquid phase sintering approach, it is expected to have glass ceramic fabrication below its melting phase with acceptable mechanical and physical properties. The ability of cullet to merge with other waste materials such as paper ash has received much attention especially to form aluminosilicate and advanced silicate-based glass-ceramics by direct sintering. However, in this method, the cullet needs to be homogenized with other components that favor crystallization due to low crystallization tendency and compositional restriction of the cullet itself [2,3]. The production of wollastonite glass-ceramic has aroused considerable interest in industrial applications such as ceramic refractories, reinforcing rods in concrete and the latest is bioactive material like implants and bone substitutes. Naturally, it is reported that the optimum composition of wollastonite is 48 wt% CaO and 52 wt% SiO_2 with some trace elements like manganese, potassium, magnesium, aluminum, iron, and sodium [4]. Few studies have been reported on wollastonite glass-ceramic made from various of waste such as mixtures of automobile waste glass and waste shell, waste glass and coal fly ash, window glass powders and F-type coal fly ash [3,5–7]. The major mineral resources of these wastes are mostly SiO_2, Al_2O_3, and CaO which could promote the formation of ceramic. However, the physical and the structure of glass-ceramic is affected by the concentration of minerals. If the amount of Al_2O_3in the mixture is more than CaO, it would favor the presence of anorthite phase and inhibited the pore generation of the glass ceramic body. On the other hand, if the amount of CaO is higher, it would break the Si–O bonds and act as modifier, thus reducing the silicate melt viscosity and consequently accelerate the growth of pores [8].

In this work, glass-ceramic from cullet-paper ash-Kaolin clay will be studied. The presence of minerals in the glass-ceramic and the sintering temperature play important roles in influencing the physical and pore structure of the ceramic.

2. Preparation procedure

The cullet is collected from Soda Lime Silica (SLS) waste container supplied by Malaya Glass Company, while

CONTACT M.R. Sahar mrahim057@gmail.com Advance Optical Material Research Group, Department of Physics, Faculty of Science, UniversitiTeknologi Malaysia, 81310 Utm, Skudai, Johor, Malaysia

paper ash is collected from an incineration paper plant (Cheras, Selangor, Malaysia) and Kaolin clay from the local market. The SLS waste containers were crushed before ball-milled by alumina balls for 48 hours and then is sieved by 100 µm sieve size to form a cullet powder. The paper ash and Kaolin clay powders are also obtained using the same procedure. A total batch of 7.0 g with the appropriate amount of powder is mixed homogeneously for 2 hours using ball mill with a stoichiometric ratio of (x) paper ash–($80 - x$) cullet–20 kaolin clay (10 wt% ≤ x ≤ 30 wt%). After that, the sample is pressed at 40 kN into a disc-shaped pellet of 4 mm in diameter. Dried pellets are then sintered at three different temperatures 900°C, 1000°C, and 1100°C with a soaking time of 2 hours. Table 1 list the nominal composition of the glass-ceramic sample.

The elemental content of raw material used was confirmed by Energy Dispersive X-Ray Analysis (EDAX, Swiftwed 3000). Table 2 shows the chemical compositions of raw materials used in the form of oxides. It reveals that cullet and Kaolin clay has an abundant of SiO_2 followed by Na_2O, Al_2O_3, and CaO. Meanwhile, paper ash contains more of CaO than $Al_2O_3$and SiO_2. The fluxing agent such as Na^+ and Ca^{2+}will promotes sintering at lower temperature and consequently reduce the energy consumption of glass-ceramic

The bulk density (ρ_{bulk}) of the sample is determined according to the Archimedes principle using Precisa XT 220A. The phase modification diffractogram is obtained from X-ray diffraction PANanalyticalX'pert PRO MRD PW3040 using a radiation source of Cu *Kα* (λ = 1.54) operating at 40 kV and 35 mA, recorded from 10–80° (2θ) with a speed of 0.05° 2θ/2.5 s. The quantitative phase analysis after **Rietveld refinement** was identified using SmartLab Studio II Powder XRD software from Rigaku. Meanwhile, the surface morphology is depicted using the Variable Pressure Scanning Electron Microscope (JEOL JSM-IT300LV) with an accelerating voltage of 10 kV. The samples are faintly platinum-coated prior to analysis to get the effective conductive surface.

Table 1. The nominal composition of glass-ceramic samples at 900°C, 1000°C and 1100°C sintering temperature.

	Composition (wt%)		
Sample No.	Cullet powder	Paper Ash	Kaolin Clay
S_1	50	30	20
S_2	55	25	20
S_3	60	20	20
S_4	65	15	20
S_5	70	10	20

Table 2. The chemical compositions of raw materials after confirmation by EDAX analysis.

Constituents (wt%)	Cullet	Paper ash	Kaolin clay
SiO_2	64.66	11.57	79.00
TiO_2	0.00	0.00	1.60
Al_2O_3	0.00	16.54	17.90
MgO	0.00	5.87	0.00
Fe_2O_3	0.14	14.90	0.40
CaO	17.04	51.12	0.20
Na_2O	17.37	0.00	0.40
K_2O	0.79	0.00	0.50
Total	100	100	100

3. Results and discussion

3.1. Bulk density

Figure 1 shows the variation of cullet content with **bulk** density. From Figure 1 it can be seen that with the increase in cullet content, the bulk density initially increases but then decreases as the cullet content is further increased. The optimum density is achieved at the ratio of cullet glass to paper ash content 55:25 while kaolin clay has remained at 20 wt %. A similar result is also reported elsewhere [9]. The density reached optimum because of vitrification between cullet glass, paper ash and kaolin clay to form liquid phase which promotes adhesion and polymerization between particles and consequently make samples more compact. In addition, the fluxing action by the alkali activation from network-modifying components such as CaO may also contributes in the increase of densification of sample and promoting the growth of wollastonite crystal [10]. However, if the cullet content is further increased beyond 55 wt %, the density starts to decrease probably due to the Si sp^3 electronic configuration that forms 3-dimensional geometric silicate structure, which is considered to be apt to form viscous layer, thus more effective in retaining gases inside the ceramic matrix, which consequently reducing the viscosity and leading to a lower particle density [6,9,11,12]. From Figure 1, it also found out that the density decreases as the sintering temperature is increased. This is probably due to the bloating effect and higher porosity which is caused by the decomposition of calcium carbonate reaction and iron oxide reduction process as [13–16],

$$CaCO_3 \rightarrow CaO + CO_2, \text{ and}$$

$$\mathbf{3Fe_2O_3 \rightarrow 2Fe_3O_4 + 0.5O_2} \quad \text{(a)}$$

$$\mathbf{2Fe_3O_4 \rightarrow 6FeO + O_2} \quad \text{(b)}$$

The reduction process of iron oxide as quoted in Equations (a) and (b) may occur simultaneously [13] where in overall, Fe^{3+} is reduced to Fe^{2+}. It should be noted out that sample with 70 wt% cullet content (sintered at 1100°C) experienced distortion which reflects the lower viscosity of the sample. Another interesting to note is that the density of the sample is below 2.0 g.cm^{-3}. This indicates that it is a type of lightweight aggregate (LWA) of glass-ceramic.

3.2. X-ray diffraction (XRD)

The XRD pattern for glass-ceramics samples under different sintered temperatures (900°C, 1000°C, and 1100°C) is shown in Figure 2. According to Figure 2, β-wollastonite

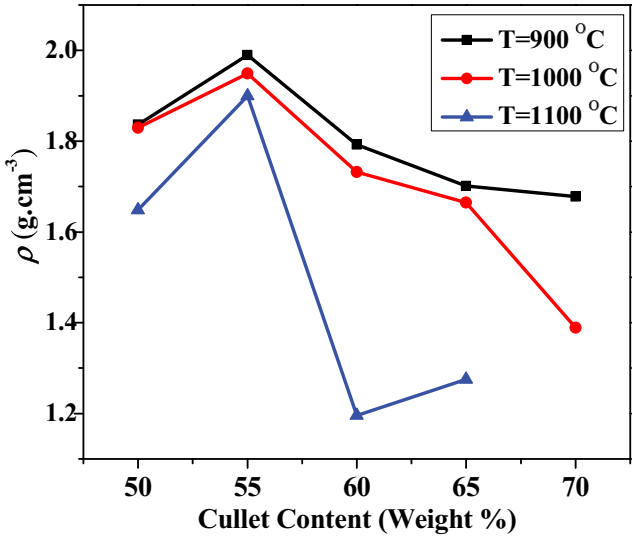

Figure 1. The variations of bulk density against cullet content of sintered glass-ceramic at different temperatures. The line is drawn for the guide to the eye only.

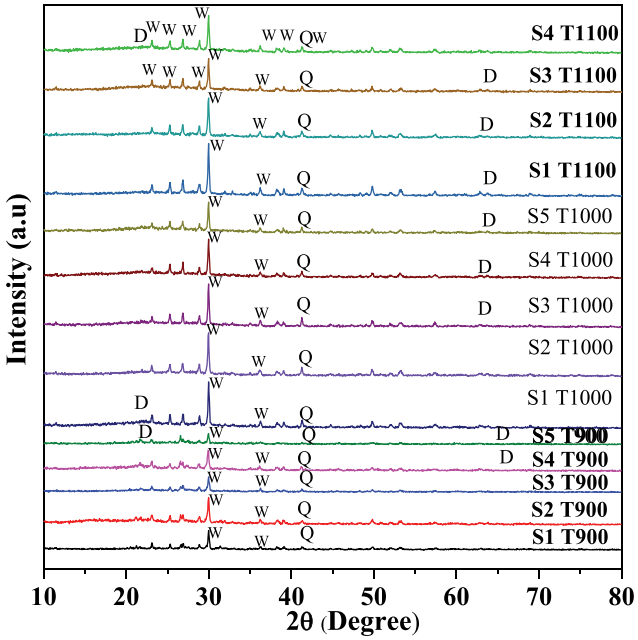

Figure 2. X-ray diffraction of all glass-ceramic samples. The peaks indicate the presence of W = Wollastonite, D = Dicalcium Silicate, and Q = quartz.

($CaSiO_3$) is present as a major phase. The minor peaks indicate the presence of γ-dicalcium silicate (Ca_2SiO_4) and quartz (SiO_2). Surprisingly, the formation of anorthite ($CaAl_2Si_2O_8$) is not been detected in the present study probably because limited contents of Al_2O_3 which inhibit its reaction with wollastonite or quartz. Furthermore, it is known that wollastonite and dicalcium silicate are remained stable up to 1100°C [14,15].

From Figure 2, it can also be seen the early formation of β-wollastonite even at 900°C. This presence is favored probably due to the presence of impurities or additives from raw materials such as Al_2O_3, MgO, $Fe_2O_3$and abundant of CaO in paper ash which may act as promoters to reduce energy consumption to form wollastonite in the lower temperature range [4,9,16–20]. The quantity of quartz in the raw materials is also influenced by the formation of wollastonite at a sintering temperature of 900°C to 1100°C. As the cullet content is further increased beyond 55 wt% (S2), the intensity of the wollastonite peaks decreases followed by an increase of few peaks of γ-dicalcium silicate or Larnite (Ca_2SiO_4) and quartz (SiO_2). Larnite is formed probably by the reaction between excessive of quartz from cullet and lime (CaO) after cooling the sample to room temperature and it is in agreement with the other work [21]. Larnite also can be formed by the reaction of wollastonite with lime at the sintering temperature of 1000°C and 1100°C [22]. The formation of wollastonite in this study can be

classified as low-temperature wollastonite (β-Wollastonite) since it is formed at a temperature less than 1125°C [23]. The reaction pathway for wollastonite and larnite formation may be written as follow [24,25];

$$CaO + SiO_2 \rightarrow CaSiO_3(\text{Wollastonite}) \quad (1)$$

$$2CaO + SiO_2 \rightarrow Ca_2SiO_4(\text{Larnite}) \quad (2)$$

$$CaSiO_3 + CaO \rightarrow Ca_2SiO_4(\text{Larnite}) \quad (3)$$

3.3. Rietveld refinement and porosity

A typical XRD pattern of **Rietveld** analysis for the sample with cullet content 55 wt% at sintering temperature 900°C is shown in Figure 3. The **Rietveld refinement** was employed to estimate the volume fraction of crystalline phase, volume dimension, crystallographic density and porosity of all glass-ceramic samples.

The evolutions of crystallinity from **Rietveld refinement** against the cullet content at different sintering temperature are presented in Figure 4. Figure 4(a–c) represents the β-Wollastonite, Larnite and quartz phase, respectively. The result delineates that the composition of cullet/paper ash and sintering temperature have greatly influenced in the formation of β-Wollastonite. The graph illustrated in Figure 4(a) shows that the β-Wollastonite phase increases progressively with the increasing of sintering temperature.

This is quite understandable as has been explain earlier. From Figure 4(b), it can be seen that the minimum contents of Larnite occurs at cullet content 60 wt % for all sintering temperature while in Figure 4(c), it can be seen that the decomposition of quartz might contribute to the formation of β-Wollastonite and Larnite. It can also further noticed that at cullet content 60 wt% for all sintering temperature, the amount of quartz is optimum while the composition of β-Wollastonite and Larniteare at minimum. However, as the sintering temperature is increased, the amount of quartz decreases down to 20 wt% at 1100°C. At this point, as the cullet content is increased, the decomposition of quartz decreases and the formation of β-Wollastoniteis replaced by the occurrence ofLarnite phase. These results demonstrated that there is no new particles are formed during sintering. This indicates the occurrence of a heterogeneous nucleation process [26]. The overall quantitative analysis results show that the optimum composition for all sintering temperature is at 55 wt% cullet, 25 wt% paper ash and 20 wt% Kaolin clay.

The increase in the volume fraction crystallinity of β-wollastonite as the temperature is increased indicates the occurrence of a reactive crystallization. Similar results have also been reported elsewhere [15,27]. As the sample is properly heated, the internal energy of the atoms will increase due to vibration which consequently changes the atomic distance or breaking some of the atomic bonds before diffuse to another atom to form new nuclei thus promoted a crystal growth with the same phase [28]. Since the Cacationmobilities are higher than Si atoms, then the phase formation of β-wollastonite is more pronounced than the unreacted quartz at higher sintering temperature. In this case, the movement of Ca^{2+} ions was accelerated and the collision along quartz rim increases, thus the crystallinity of β-wollastonite increases as-sintered temperatures is increased [14,19,29–31].

The crystal cell parameters of $CaSiO_3$ (Wollastonite), Ca_2SiO_4 (Larnite) and SiO_2 (Quartz) which are used as initial values for Rietveld refinement are shown in Table 3. The accurate parameters used for Rietveld refinement are crucial to ensure the persistent of refinement of crystallization [32–34]. The theoretical density, ρ_{th} for the sample consisting of mixed solid phase can be estimated using a relation [35],

$$\rho_{th} = \sum (\text{volume fraction of each crystalline phase}).(\rho_{cr}\text{of each crystalline phase}) \quad (4)$$

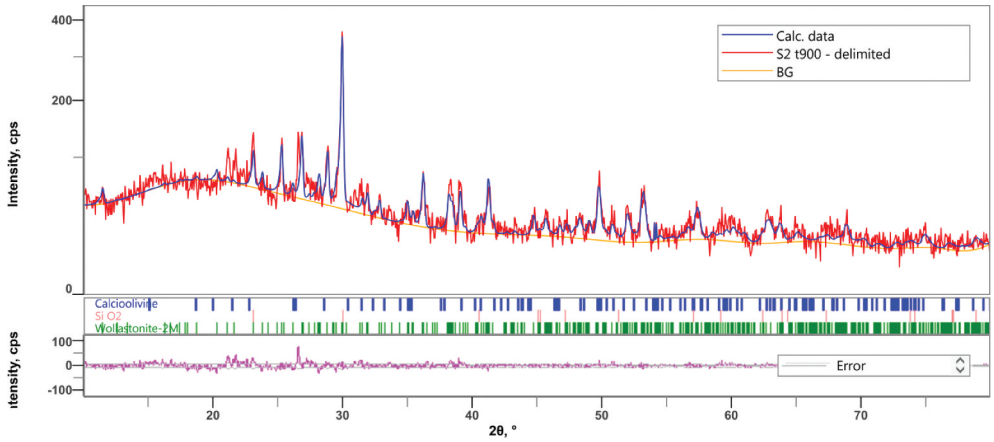

Figure 3. XRD patterns of **Rietveld** analysis on the sample with 55 wt% cullet content for sintering temperature at 900°C.

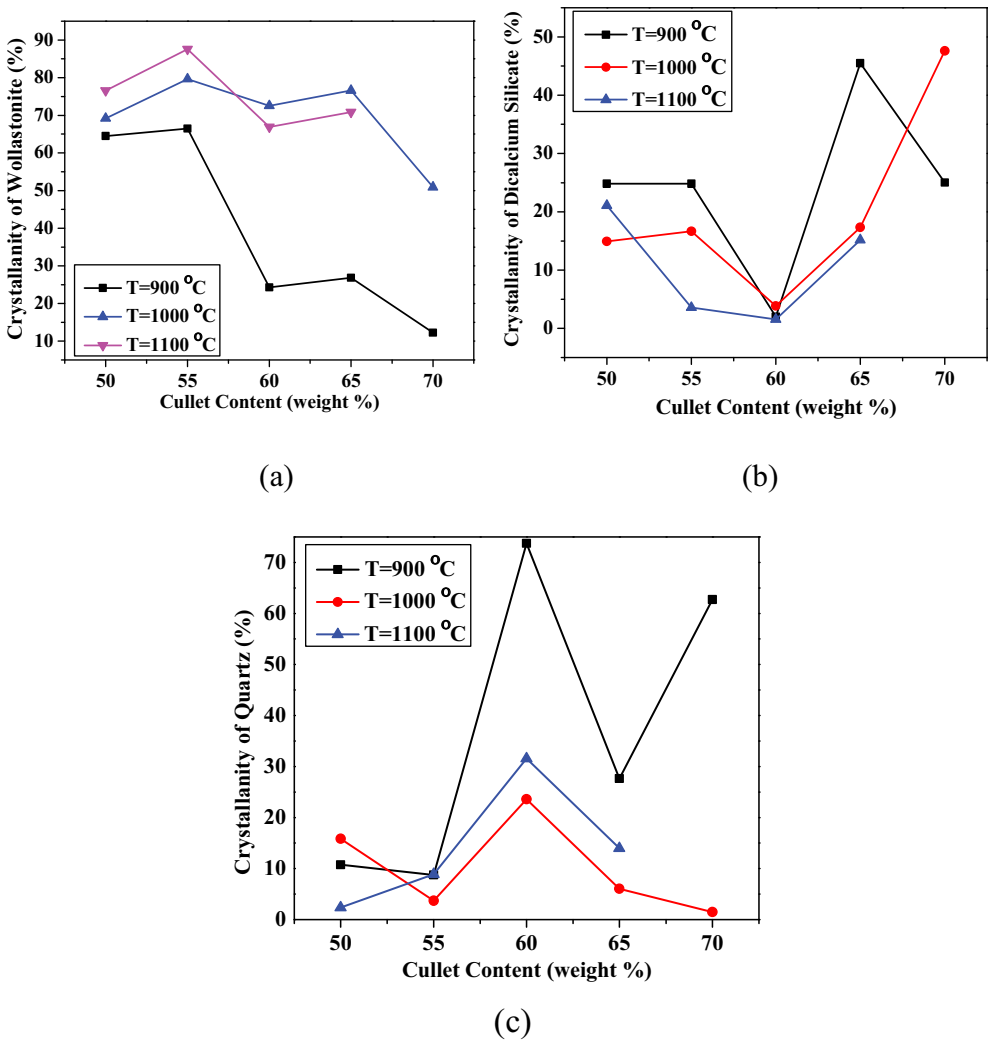

Figure 4. Evolution of crystallinity (%) phases at different temperature 900°C, 1000°C, and 1100°C in (a) β-wollastonite (b) Dicalcium silicate and (c) Quartz.

Table 3. Lattice parameters of $CaSiO_3$ (Wollastonite), Ca_2SiO_4 (Dicalcium Silicate) and SiO_2 (Quartz) in COD database.

Phase	*a*(Å)	*b*(Å)	*c*(Å)	*α*	*β*	*γ*	V(Å)	*Crystallography Density, ρ_{cr}*(gcm^{-3})	Crystal System	Space group	Z
$CaSiO_3$	15.426	7.3200	7.0660	90	95.30	90	794.34	2.91	Monocilinic	P 1 21/a	12
Ca_2SiO_4	5.0762	11.2136	607,583	90	90	90	384.70	2.9	Orthohombic	P b n m	4
SiO_2	4.9650	4.9650	5.4240	90	90	120	115.79	2.58	Hexagonal	P 31 2 1	3

where $\boldsymbol{\rho_{cr}}$**(g/cm^3)**, is the crystallographic density which can be obtained using,

$$\rho_{cr} = \frac{ZM}{NV} \tag{5}$$

where *Z* is the atomic number in a unit cell, *M* is the molecular weight of each compound, *N* is Avogadro's number and *V* is calculated the volume of a unit cell [36–38]. Meanwhile, the porosity of the pressed sample, P can be estimated using the relation [35];

$$P\% = 100 - \left(\frac{\rho_{bulk}}{\rho_{th}}\right)\% \tag{6}$$

Notwithstanding, there are few limitations using this theory since it could not reach all pores and some closed pores which could not be considered in the calculations. Then, it could give higher value of porosity since theoretical density from XRD measurements was not involved in any amorphous phases that present in the samples and only reach certain pore sizes depending on the radius of the molecule used [39].

Table 4 shows the porosity of each sample at different sintering temperatures. From Table 4, it can clearly be observed that the volume fraction of the sample decreases as temperature is increased. This is quite understandable since as the temperature is increased, the interatomic bonding decreases, thus the volume generally decreases. Meanwhile, the relationship between bulk density and porosity of the sample can be made and is shown in Figure 5. From Figure 5, it can clearly be observed that the experimental density decreases

Table 4. Volume fraction of $CaSiO_3$, $Ca_2SiO$and SiO_2, theoretical densities, bulk density and porosity of the sample.

Sample	Volume fraction of $CaSiO_3$ (%)	Volume fraction of Ca_2SiO_4 (%)	Volume fraction of SiO_2 (%)	Theoretical Density, ρ_{th} (±0.01 g/cm3)	Bulk density, ρ_{bulk} (±0.01 g/cm3)	ρ_{bulk}/ρ_{th} (%)	Porosity (%)
T900							
S1	66.09	25.68	8.22	2.83	1.84	64.90	35.10
S2	92.51	22.41	23.39	2.85	1.99	69.70	30.30
S3	19.75	29.63	50.62	2.84	1.79	63.05	36.95
S4	52.8	39.96	27.24	2.78	1.70	61.15	38.85
S5	37.04	34.59	28.36	2.81	1.68	59.67	40.33
T1000							
S1	64.17	19.97	15.86	2.87	1.83	63.75	36.25
S2	75.88	22.96	11.16	2.92	1.95	66.76	33.24
S3	55.54	26.41	18.04	2.87	1.73	60.43	39.57
S4	24.14	16.65	69.21	2.69	1.67	62.00	38.00
S5	7.52	5.34	87.13	2.63	1.39	52.91	47.09
T1100							
S1	60.00	15.69	24.31	2.84	1.65	58.06	41.94
S2	71.03	25.25	23.72	2.91	1.90	65.23	34.77
S3	53.50	12.82	33.70	2.81	1.20	42.60	57.40
S4	29.60	8.64	61.76	2.71	1.27	47.02	52.98

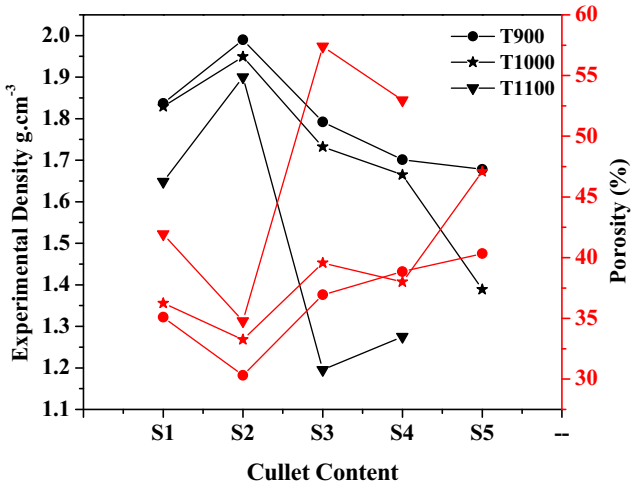

Figure 5. Density and porosity patterns of glass-ceramic samples as a function of composition and sintering temperature.

Table 5. Lattice parameters and cell volume refinement of major phase $CaSiO_3$ (Wollastonite).

Sample	a (Å)	b(Å)	c(Å)	β(°)	V_o (Å^3)
T900					
S1	15.4321	7.3199	7.0617	95.32	794.271
S2	15.4440	7.3256	7.0664	95.31	796.047
S3	15.4484	7.3275	7.0698	95.31	796.858
S4	15.4540	7.3228	7.0653	95.32	796.126
S5	15.4853	7.3445	7.0710	95.42	800.601
T1000					
S1	15.4172	7.3068	7.0482	95.38	790.486
S2	15.4168	7.3153	7.0580	95.33	792.555
S3	15.4632	7.3316	7.0733	95.44	798.307
S4	15.4796	7.3261	7.0717	95.35	798.481
S5	15.4334	7.2989	7.0455	95.43	790.091
T1100					
S1	15.4145	7.3174	7.0565	95.43	792.369
S2	15.4439	7.3253	7.0675	95.27	796.175
S3	15.4294	7.3234	7.0648	95.35	794.813
S4	15.4180	7.3132	7.0502	95.47	791.325

as the porosity increases. It is also shown that the minimum porosity occurs at cullet content 55 wt% but increases as the cullet content is increased. It can also be noted out that the porosity increases as the sintering temperature is increased.

Table 5 summarizes Reitveld refinement results of major phase Wollastonite at three different sintering temperatures. The results show that there are slight discrepancies of the calculated lattice parameter values by **Rietveld refinement** to the literature values as in Table 3. This is due to a limit on the degree of anisotropy of thermal motion or isotropic vibration that could lead to the expansion of the Si-O bond to become prominent [40]. Besides that, another factor that contributes to these fluctuations is probably due to the order-disorder phase transition and rearrangement of cations in the crystallite glass-ceramic [33]. Furthermore, anion vacancies from perovskites structure of $CaSiO_3$, small cation interstitials within Si, Ca and O and impurities from waste material probably affect the expansion or contraction of the unit cell that may cause the discrepancy in the lattice parameters [41–44].

The effect of sintering temperature on the porosity can be seen clearly in Figure 6. From Figure 6, it can be seen that at 900°C the sample begins to softened, the

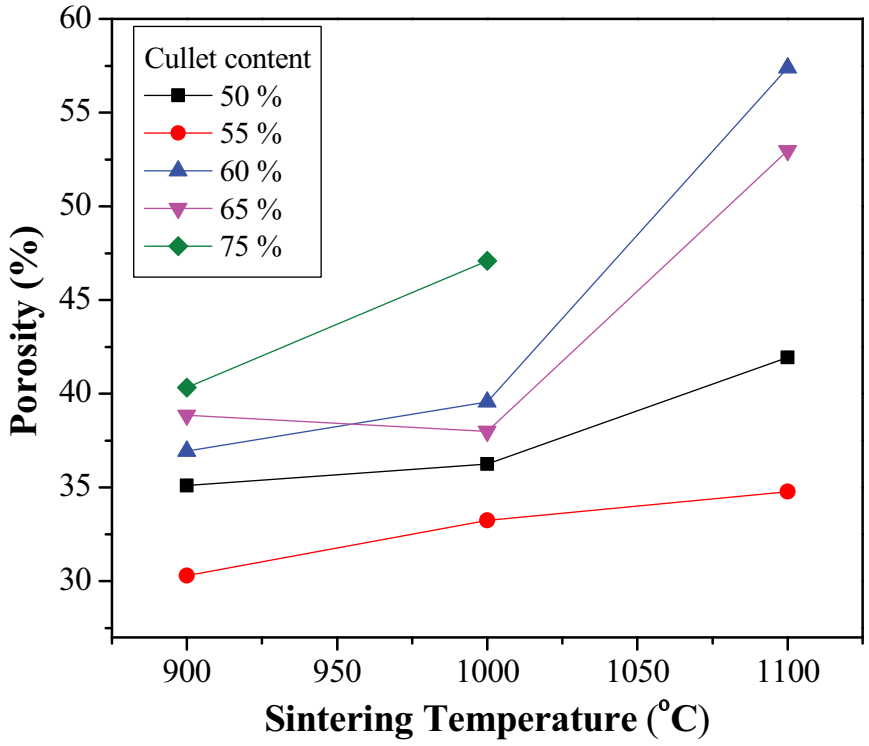

Figure 6. Porosity as a function of Sintering Temperature.

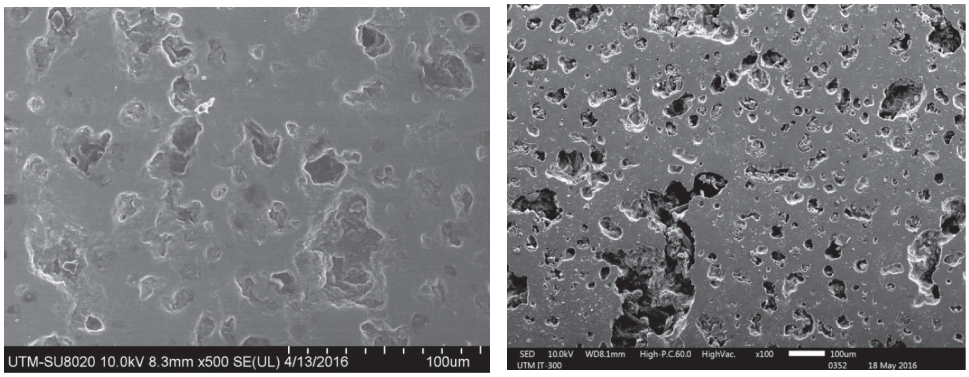

(a) T900

(b) T1000

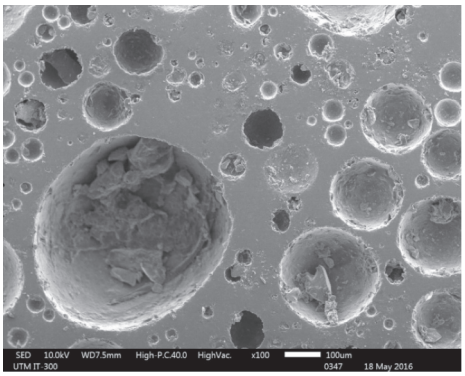

(c) T1100

Figure 7. The surface morphology of glass-ceramic contains 55 wt% cullet content sintered at (a) 900°C (b) 1000°C and (c) 1100°C.

gases are released due to the decomposition of calcite to lime and carbon dioxide. At this stage, the pore structure started to form with fine pore size distributions [45]. With the increase of sintering temperature from 1000°C to 1100°C, these pores became larger which indicates the increase of porosity. This perhaps is due to decomposition of ferrite ion in paper ash and cullet from Fe^{3+} to Fe^{2+} ions and also by the decrement of liquid phase viscosity which leads to the capture of more gasses and enhance the pore size growth [8,45,46].

3.4. Scanning electron microscope (SEM)

Figure 7 shows SEM images of the sample with 55 wt% of cullet at sintering temperature 900°C, 1000°C and 1100°C. At low sintering temperature 900°C (Figure 7 (a)), it can be seen the intergranular pores of varieties in shape and sizes with a smooth surface which might be resulting from the softened sample along with wrapped gasses during the decomposition of calcite. Further increasing the temperature to 1000°C (Figure 7 (b)) the intergranular pores increase in size with a more glassy surface. Lastly, at sintering temperature of 1100° C (Figure 7(c)), it can be seen that the intragranular semispherical pores are bigger in size. This is due to the intragranular-induced crystallization pores that growth along the surface [47,48]. From Figure 7, it can also be said that the mixture of wastes from paper ash and cullet glass containing a large amount of calcium carbonate and ferrous ion could bear for the development of porous glass-ceramic. Thus, it can be said that a close pore glass-ceramic which may be applicable for building insulation application, can suitably be obtained via the composition of 55 wt% cullet and 25 wt% paper ash sintered at 900°C.

4. Conclusion

The synthetic wollastonite glass-ceramic has successfully been synthesized from cullet, paper ash and kaolin clay using solid state reaction. By increasing the sintering temperature to 1100°C, the porosity is found to increase and the density is decreased, probably due to more bloating gas trapped in the glass-ceramic matrix. SEM analysis at low sintered temperature showed the occurrence of intergranular pores with varieties of shapes and sizes with a smooth surface. As the sintering temperature is increased the intragranular semispherical pores with bigger sizes take place. The composition of a wollastonite glass-ceramic sample containing 55 wt % of cullet, 25 wt% paper ash and 20 wt% of Kaolin clay sintered at 900°C gives the optimum properties suitable for building materials.

Acknowledgments

The authors gratefully acknowledge this work was supported by the [Ministry of Higher Education of Malaysia, Universiti Teknologi Malaysia] under Grant [number 08H42] and [number 4F752]. The authors would also like to thank NorshilaJarkoni, SitiAmlahMohdAzmi, SitiAisyahJupri, SyariffahNurathirah Syed Yaacob, Hamiza Ahmad Tajuddin, NurhafizahHasim, PuziAnigrahawati, and EzzaSyuhada for contribution and supports for this study.

Disclosure statement

No potential conflict of interest was reported by the authors.

Funding

This work was supported by the Universiti Teknologi Malaysia [4F752]; Universiti Teknologi Malaysia [08H42].

ORCID

K. Abu-Samah http://orcid.org/0000-0002-2723-3803

References

[1] Samori Z, Khairudin Z, Saedon R, et al. Sustainable waste management via incineratin system: an Islam Outlook for conservation of the environment. J Fundam Appl Sci. 2017;9:538–557.
[2] Ponsot I, Detsch R, Boccaccini AR, et al. Waste derived glass ceramic composites prepared by low temperature sintering/sinter-crystallisation. Adv Appl Ceram. 2015;114:S17–S25.
[3] Yi W, Gao H, Xu Y. Sintering and reactive crystal growth of diopside – albite glass – ceramics from waste glass. J Eur Ceram Soc. 2011;31:1669–1675.
[4] Zhu L, Sohn HY. Growth of 2M-wollastonite polycrystals by a partial melting and recrystallization process for the preparation of high-aspect-ratio particles. J Ceram Sci Technol. 2012;3:169–180.
[5] Yoon S, Lee J, Lee J, et al. Characterization of wollastonite glass-ceramics made from waste glass and coal fly ash. J Mater Sci Technol. 2013;29:149–153.
[6] Wei Y, Cheng S, Ko G. Effect of waste glass addition on lightweight aggregates prepared from F-class coal fly ash. Constr Build Mater. 2016;112:773–782.
[7] Wei Y, Cheng S, Ou K, et al. Effect of calcium compounds on lightweight aggregates prepared by firing a mixture of coal fly ash and waste glass. Ceram Int. 2017;43:15573–15579.
[8] Zhou M, Ge X, Wang H, et al. Effect of the CaO content and decomposition of calcium-containing minerals on properties and microstructure of ceramic foams from fly ash. Ceram Int. 2017;43:9451–9457.
[9] Heriyanto, Pahlevani F, Sahajwalla V. Synthesis of calcium silicate from selective thermal transformation of waste glass and waste shell. J Clean Prod. 2018;172:3019–3027.
[10] Luo Y, Ma S, Zheng S, et al. Mullite-based ceramic tiles produced solely from high-alumina fl y ash: preparation and sintering mechanism. J Alloys Compd. 2018;732:828–837.

[11] Qing Z, Zhou W, Xia W, et al. Crystallization kinetics, sintering, microstructure, and properties of low temperature co- fi red magnesium aluminum silicate glass-ceramic. J Non Cryst Solids. 2018;486:14–18.
[12] Bernardo E, Bontempi E, Depero L, et al. Recycling of pre-stabilized municipal waste incinerator fl y ash and soda-lime glass into sintered glass-ceramics. J Clean Prod. 2015;89:224–230.
[13] Monazam ER, Breault RW, Siriwardane R. Reduction of hematite (Fe2O3) to wüstite (FeO) by carbon monoxide (CO) for chemical looping combustion. Chem Eng J. 2014;242:204–210.
[14] Riccardi MP, Messiga B, Duminuco P. An approach to the dynamics of clay firing. Appl Clay Sci. 1999;15:393–409.
[15] Zhang W, Liu H. A low cost route for fabrication of wollastonite glass-ceramics directly using soda-lime waste glass by reactive crystallization-sintering. Ceram Int. 2013;39:1943–1949.
[16] Nour WMN, Mostafa AA, Ibrahim DM. Recycled wastes as precursor for synthesizing wollastonite. Ceram Int. 2008;34:101–105.
[17] Trindade MJ, Dias MI, Coroado J, et al. Mineralogical transformations of calcareous rich clays with fi ring : A comparative study between calcite and dolomite rich clays from Algarve, Portugal. Appl Clay Sci. 2009;42:345–355.
[18] Taylor JR, Dinsdale AT. Thermodynamic and phase diagram data for the CaO-SiO2 system. Calphad. 1990;14:71–88.
[19] Lu J, Cong X, Lu Z. Influence of magnesia on sinter-crystallization, phase composition and flexural strength of sintered glass-ceramics from waste materials. Mater Chem Phys. 2016;174:143–149.
[20] Chinnam RK, Bernardo E, Will J, et al. Processing of porous glass ceramics from highly crystallisable industrial wastes. Adv Appl Ceram. 2015;114:11–16.
[21] Bohme N, Hauke K, Neuroth M, et al. In situ Raman imaging of high-temperature solid-state reactions in the CaSO 4 – siO 2 system. Int J Coal Sci Technol. 2019;6:247–259.
[22] Obeid MM. Crystallization of synthetic wollastonite prepared from local raw materials. Int J Mater Chem. 2014;4:79–87.
[23] Mazzucato E, Gualtieri A. Wollastonite polytypes in the CaO-SiO2 system. Phys Chem Miner. 2000;27:565–574.
[24] Wang Y, Shih K, Jiang X. Phase transformation during the sintering of g -alumina and the simulated Ni-laden waste sludge. Ceram Int. 2012;38:1879–1886.
[25] Moreno-maroto JM, González-corrochano B, Alonso-azcárate J, et al. Assessment of crystalline phase changes and glass formation by Rietveld- XRD method on ceramic lightweight aggregates sintered from mineral and polymeric wastes. Ceram Int. 2018;44:11840–11851.
[26] Chang C, Jean J. Crystallization kinetics and mechanism of low-dielectric, low-temperature, cofirable CaO–B2O3–SiO2 glass-ceramics. J Am Ceram Soc. 1999;32:1725–1732.
[27] Wei SI, Chao D. An investigation on crystallization property, thermodynamics and kinetics of wollastonite glass ceramics. J Cent South Univ. 2018;25:28.
[28] Ratnawulan, Fauzi A, Sukma HA. Effect of calcination temperature on phase transformation and crystallite size of copper oxide (CuO) powders. AIP Conf Proc. 2017;1868:060091–060095.
[29] Day SJ, Thompson SP, Evans A, et al. Thermal processing and crystallization of amorphous Mg-Ca silicates. Meteorit Soc. 2013;48:1459–1471.
[30] Hossain SKS, Roy PK. Study of physical and dielectric properties of bio- waste derived synthetic wollastonite. J Asian Ceram Soc. 2018; 6(3); 289–298.
[31] Zhao S, Gao J, Ma S, et al. Mechanism and modelling of reactive crystallization process of lithium carbonate. J Process. 2019;7:248.
[32] Shu X, Tian Y, Song G, et al. Thermal expansion and theoretical density of 2,20,4,40,6,60-hexanitrostilbene. J Mater Sci. 2011;46:2536–2540.
[33] Yasukawa K, Terashi Y, Nakayama A. Crystallinity analysis of glass-ceramics by the Rietveld method. J Am Ceram Soc. 1998;81:2978–2982.
[34] Kemethmu S, Roosen A. Quantitative analysis of crystalline and amorphous phases in glass– ceramic composites like LTCC by the Rietveld method. J Am Ceram Soc. 2006;89:2632–2637.
[35] Richerson DW, Lee WE. Modern ceramic engineering properties, processing, and use in design. 4th ed. Boca Raton (Florida): CRC Press; 2018.
[36] Slatineanu T, Raluca A, Nicolae M, et al. Synthesis and characterization of nanocrystalline Zn ferrites substituted with Ni. Mater Res Bull. 2011;46:1455–1460.
[37] Santos TH, Grilo JPF, Loureiro FJA, et al. Structure, densification and electrical properties of Gd3+and Cu2+co-doped ceria solid electrolytes for SOFC applications: effects of Gd2O3content. Ceram Int. 2018;44:2745–2751.
[38] Abdul Halim DNF Effect of sintering on microstructure and complex permittivity of magnesium titanate doped barium strontium titanate prepared via mechanical alloying [PhD Thesis]. Malaysia (selangor): Universiti Putra Malaysia; 2018.
[39] Unosson JE, Persson C, Engqvist H. An evaluation of methods to determine the porosity of calcium phosphate cements. J Biomed Mater Res B Appl Biomater. 2015;103B:62–71.
[40] Taylor D. The thermal expansion behaviour of the framework silicates. Mineral Magn. 1972;38:593–604.
[41] Sebastian MT. Zirconium tin titanate. 1st ed. Amsterdam (The Netherlands): Elsevier; 2008. p. 83–108.
[42] Babu SS, Specht ED, David SA, et al. In-situ observations of lattice parameter fluctuations in austenite and transformation to bainite. Metall Mater Trans A. 2005;36A:3281–3289.
[43] Khan S, Kaushik SD, Verma A, et al. Lattice parameter instabilities during multi-phase precipitation in Alloy 693. J Alloys Compd. 2017;700:149–154.
[44] Krawitz A, Sinclair R, Steel I, et al. On the lattice parameter of non- random solid solutions. Philos Mag. 1975;31:697–712.
[45] Liu T, Tang Y, Li Z, et al. Red mud and fly ash incorporation for lightweight foamed ceramics using lead-zinc mine tailings as foaming agent. Mater Lett. 2016;183:362–364.
[46] Liu T, Lin C, Liu J, et al. Phase evolution, pore morphology and microstructure of glass ceramic foams derived from tailings wastes. Ceram Int. 2018;44:14393–14400.
[47] German R. Liquid phase sintering. Troy (New York): Springer Science and Business Media New York; 1985.
[48] Karamanov A, Pelino M. Induced crystallization porosity and properties of sintereds diopside and wollastonite glass-ceramics. J Eur Ceram Soc. 2008;28:555–562.